The
University
Of
Sheffield.

This is a repository copy of *High-strength steel wires containing corrosion pits : stress analysis and critical distance based fatigue life estimation*.

White Rose Research Online URL for this paper:
http://eprints.whiterose.ac.uk/152799/

Version: Accepted Version

White Rose
university consortium
Universities of Leeds, Sheffield & York

eprints@whiterose.ac.uk
https://eprints.whiterose.ac.uk/

High-strength steel wires containing corrosion pits: stress analysis and critical distance based fatigue life estimation

Zhiyu Jie[1] and Luca Susmel[2]

[1]Department of Civil Engineering, Ningbo University, Ningbo 315211, China

[2]Department of Civil and Structural Engineering, The University of Sheffield,

Sheffield S1 3JD, UK

<u>Corresponding Author</u>:   Prof. **Luca Susmel**
Department of Civil and Structural Engineering
The University of Sheffield, Mappin Street, Sheffield, S1 3JD, UK
Telephone: +44 (0) 114 222 5073
Fax: +44 (0) 114 222 5700
E-mail: l.susmel@sheffield.ac.uk

Abstract

The present paper deals with the problem of assessing the fatigue lifetime of high-strength steel wires containing corrosion pits, with this investigation being based on a large number of experimental data selected from the technical literature. To evaluate the stress concentration phenomena characterising corroded metallic wires, according to the state-of-the-art knowledge, pits were modelled either as semi-ellipsoidal cavities or as hemispherical notches. The stress concentration factors, K_t, associated with these simplified pit geometries were calculated numerically by solving numerous three-dimensional FE models. Subsequently, the K_t values being determined according to this standard numerical procedure were post-processed systematically to derive simple analytical solutions suitable for estimating, in situations of engineering interest, the stress concentration factors associated with pitting corrosion. Finally, after making some assumptions to derive the necessary fatigue properties, the Theory of Critical Distances was used in the form of the Point Method and the Line Method to re-analyse the literature data being collected. This systematic validation exercise allowed us to prove that the Theory of Critical Distances is successful also in assessing the fatigue lifetime of high-strength metallic cables containing corrosion pits, with the obtained estimates falling within an error factor of 3. Therefore, as far as wires weakened by corrosion pits are concerned, it was demonstrated that the Theory of Critical Distances can be used to post-process the local linear-elastic stress fields when they are not only determined numerically, but also estimated by using those standard analytical solutions which are strictly valid solely for conventional notches.

Keywords: lifetime estimation; steel wires; corrosion pits; Theory of Critical Distance

Nomenclature

d   pit depth

k   negative inverse slope

l   pit length

w   pit width

A, B   fatigue constants in the L_M vs N_f relationship

D   wire diameter

E   Young's modulus

K_{Ic} plane strain fracture toughness

K_t stress concentration factor

L   critical distance value in the high-cycle fatigue regime

L_M critical distance value in the medium-cycle fatigue regime

N_o reference number of cycles to failure in the high-cycle fatigue regime

N_f number of cycles to failure

$N_{f,e}$ estimated number of cycles to failure

N_S reference number of cycles to failure in the low-cycle fatigue regime

O, r, θ polar coordinates

XYZ   external coordinates

R   load ratio ($\sigma_{min}/\sigma_{max}$)

ν   Poisson's ratio

σ_a stress amplitude

σ_{max} maximum stress in the fatigue cycle

σ_{min} minimum stress in the fatigue cycle

σ_{UTS} ultimate tensile strength

ΔK_{th} threshold value of the stress intensity factor range

$\Delta\sigma_{eff}$ range of the effective stress

$\Delta\sigma_{nom}$ axial nominal stress

$\Delta\sigma_y$ range of the local linear-elastic stress parallel to axis y

$\Delta\sigma_o$ fatigue limit range or endurance limit range at N_o cycles to failure

$\Delta\sigma_1$ range of the local linear-elastic maximum principal stress

1. Introduction

High-tensile steel cables are widely used in the construction of large structures such as, for instance, long-span bridges. However, the mechanical properties of steel wires are very sensitive to corrosion as well as to the presence of those defects that are usually introduced during manufacturing. In particular, the overall fatigue strength of metallic cables is seen to decrease as a consequence of the fact that corrosion and pre-existing superficial defects can not only reduce the cross-sectional area significantly, but also cause very severe localised stress concentration phenomena[1].

As far as corrosion is concerned, local pits are seen to act as sharp geometrical features that reduce markedly the strength of steel cables. This explains the reason why pitting corrosion is usually considered to be more detrimental than uniform/general corrosion.

If attention is focussed on pitting, the presence of an aggressive environment leads to the formation on the steel wires' surfaces of cavities having different shape[2]. In this context, the simplest assumption that can be made to assess the detrimental effect of corrosion pits is modelling them as hemispherical notches[3, 4]. More realistic geometrical configurations may also include bullet shapes[5, 6] and hemi-ellipsoidal cavities[7, 8]. However, independently of their profile, the reference parameters that are commonly used to characterise the geometry/shape of corrosion pits are depth, width, and aspect ratio (which is defined as the ratio between depth and width).

As mentioned earlier, the presence of pits results in localised stress concentration phenomena that can be quantified accurately provided that geometry and dimensions of the specific type of pits being analysed are described and modelled correctly. In this context, examination of the state of the art shows that, in recent years, systematic analytical and numerical work has been done to quantify, under uniaxial loading, the stress concentration factor (SCF) associated with three-dimensional hemispherical and semi-ellipsoidal pits (see, for instance, Huang et al.[9] and references reported therein). From a practical point of view, the interest in modelling both hemispherical and semi-ellipsoidal pits is due to the fact that these are the most common shapes being observed in situations of practical interest[10]. Clearly, in this specific ambit, hemispheres and semi-ellipsoids are geometrical models that are used to attempt to capture and model in a simplified way a reality which is, by nature, far more complex.

In this context, Cerit[11, 12] quantified the stress concentration effect as a function of depth, diameter, and orientation of semi-ellipsoidal pits and proposed an empirical equation that correlates the SCF, K_t, with the pit size. This empirical relationship was obtained by post-processing systematically numerous Finite Element (FE) models. The most relevant conclusion from this investigation was that, in the presence of semi-ellipsoidal pits, the aspect ratio is the main

parameter influencing the value of the SCF. Huang et al.[9] determined the SCFs in a cylindrical shaft containing pits, with this being done by numerically modelling the pits as three-dimensional semi-ellipsoidal cavities. These numerical analyses allowed them to show that, in the presence of semi-ellipsoidal pits, the SCF value varies as depth and diameter of the pit change. In a similar way, Ji et al.[13] assessed the effect of depth, width, and aspect ratio on the SCFs associated with elliptical pits, with this being done again by post-processing a large number of 3D FE models. An et al.[14] focussed their attention instead on plates containing corrosion pits. Their stress analyses showed that the pit aspect ratio and the pit depth/plate thickness ratio are the two key factors affecting the value of the SCFs associated with this specific geometrical configuration.

This brief review of the state of the art suggests that much work has already been done to quantify the values of the SCFs in large structural components/details containing corrosion pits. In contrast, very little research work has been carried out so far to quantify the stress concentration phenomena resulting from corrosion pits in steel wires. This represents one of the novel aspects that are addressed in the present paper.

Turning to the mechanical behaviour of structural components subjected to in-service time-variable loading, it is well known that the overall fatigue performance of metallic materials is markedly affected by those stress concentration phenomena arising from conventional notches. To model the detrimental effect of geometrical features of all kinds on the fracture and fatigue behaviour of metallic materials, in his well-known book[15] David Taylor recommends using the so-called Theory of Critical Distances (TCD). One of the key advantages of the TCD is that it assesses the presence of stress raisers by directly post-processing simple linear-elastic FE analyses. Thanks to its specific features, the TCD is suitable for predicting fatigue lifetime of notched components not only in the high-cycle[15], but also in the medium-cycle fatigue regime[16, 17]. Further, it can be used also to perform the fatigue assessment of notched metallic components at elevated temperatures, with this being done by keeping performing the required stress analysis by adopting a simple linear-elastic constitutive law[18]. The TCD has been proven to be capable of quantifying also the detrimental effect of other small features such as, for instance, surface roughness[19, 20] and manufacturing defects[22-24]. By taking as a starting point the pivotal work done by Susmel and Taylor[24-27], Liu and Yan[28] proposed a new multiaxial notch fatigue life prediction method based on the TCD, with the accuracy of this approach being checked against a large number of experimental results. Zhou et al.[29] used the TCD to perform the fatigue assessment of orthotropic steel decks, whereas Gorouhi[30] investigated the accuracy of the TCD in assessing the fatigue strength of those riveted structural details that are commonly employed in bridges. In parallel, Taylor et al.[31], Susmel et al.[32-34] and Karakaş et al.[35] demonstrated that the TCD is also

4

successful in estimating fatigue damage in welded joints made of steel, aluminium alloys, and magnesium alloys.

Given the complex scenario as described above, in the present paper, initially a large number of fatigue results generated by testing high-strength steel wires containing not only corrosion pits, but also semi-elliptical cracks were collected from the technical literature[36-43]. Subsequently, the SCFs in wires weakened by semi-ellipsoidal and hemispherical corrosion pits were determined numerically, with this being done by varying the ratio both between depth and width and between depth and wire diameter. An empirical equation suitable for estimating SCFs in pitted wires was determined by using the least squares method to post-process the numerical results being obtained. Finally, the accuracy and reliability of the TCD applied in the form of the Point Method and the Line Method in estimating fatigue lifetime of steel wires containing both semi-elliptical cracks and corrosion pits were checked systematically against the literature data being collected. To conclude, it should be pointed out here that the TCD was applied by determining the required local linear-elastic stress fields both by post-processing FE models solved using commercial code ANSYS® and by taking full advantage of the analytical solution proposed by Glinka and Newport[44]. Such a validation exercise allowed us to demonstrate that the TCD is successful also in predicting the fatigue lifetime of high-strength wires weakened either by corrosion pits or by superficial defects by always reaching a remarkable level of accuracy.

2. Stress concentration factors in steel wires containing corrosion pits

Examination of the state of the art[36-40] shows that the shapes of corrosion pits (Fig. 1a) are usually simplified by modelling them either as semi-ellipsoids (Fig. 1b) or as hemispheres (Fig. 1c). Given these two reference geometries, in the present investigation depth is denoted as d, length as l, and width as w, with length l and width w being parallel and perpendicular, respectively, to the direction along which the loading is applied (see also Fig. 1).

By performing a systematic data mining exercise, we selected from the technical literature a large number of fatigue results generated by testing high-strength steel wires containing corrosion pits. The data being collected are summarised in Tables 1 to 4, with the meaning of the used symbols being explained in Fig. 1. For the stress analysis exercise being performed, these experimental results were used to define the ranges of interest for the reference dimensions (i.e., l, d, w, and D) characterising those corrosion pits that are usually found in metallic wires. In particular, for the hemispherical cavities the considered values for the d-to-D ratio ranged from 0.026 up to 0.109, with d/l being clearly invariably equal to 0.5. For the semi-ellipsoids instead, ratio d/D ranged from 0.026 up to 0.12 and ratio d/l from 0.041 up to 0.276.

The reference chemical composition for those high-strength steels that are commonly used to manufacture wires is as follows[40, 41]: C (0.85~0.90%), Si (0.12~0.32%), Mn (0.60~0.90%), Cr (0.10~0.25%), S, and Cu. Given this standard chemical composition, the mechanical behaviour of high-strength steel for wires was modelled numerically by setting Young's Modulus, E, equal to 210000 MPa and Poisson's ratio, ν, to 0.3.

FE simulations were run using commercial software ANSYS®. Steel wires with a length of 100 mm and containing cavities of various shape (i.e., hemispherical or semi-ellipsoidal) and dimensions were modelled by employing three-dimensional 10-node tetrahedral structural solid elements (Fig. 2a). In the linear-elastic FE simulations, the pitted wires being analysed were loaded by applying a nominal gross tensile stress equal to 1 MPa. In any of the FE models being solved the mesh was gradually increased until convergence occurred. Figure 2 shows some examples of the stress distributions that were obtained according to the FE based procedure briefly described above. In total, we solved 32 different FE models and the obtained solutions were used to determine how K_t varies as profile and size of the corrosion pits change.

According to the examples reported in Fig. 2, in the hemispherical pits the maximum stress was seen to be on the wire surface at the edge of the pit mouth (Fig. 2b). In contrast, in the presence of semi-ellipsoidal pits the maximum stress was seen instead to be invariably at the bottom of the cavities (Fig. 2c).

In order to check whether other existing tools could be used to somehow estimate K_t in pitted wires, initially, the FE models being solved were employed to assess the accuracy of some existing analytical solutions that were obtained by considering different geometrical configurations.

According to the symbols used in the present paper, the SCF for a spherical cavity in a finite-radius cylinder under uniform remote tension can be estimated as follows[45]:

$$K_t = \frac{(27-15\nu)/(14-10\nu)}{1-\frac{4-5\nu}{7-5\nu}\cdot\frac{(2d)^3}{D^3}-\frac{3}{7-5\nu}\cdot\frac{(2d)^5}{D^5}} \tag{1}$$

According to the diagram reported in Fig. 3a, the use of Eq. (1) resulted in estimates that were surprisingly accurate, with a maximum error (in the considered dimensional interval) of about 6%.

As far as semi-ellipsoidal pits are concerned, initially the associated SCF values were attempted to be estimated by using the following relationships that are strictly valid for the case of an elliptical notch in a plate loaded in tension[8, 46]:

$$K_t = 1 + 4\frac{d}{l} \tag{2}$$

$$K_t = \frac{1+6.6\frac{d}{l}}{1+2\frac{d}{l}} \tag{3}$$

As per the chart of Fig. 3b, the use of Eq. (2) and Eq. (3) to model the case of semi-ellipsoidal pits returned very poor results, with the predictions being systematically non-conservative. Thus, an *ad hoc* formula was derived in order to devise a tool suitable for estimating analytically the SCFs in the presence of semi-ellipsoidal cavities. This formula was obtained by assuming a non-linear relationship between d/D and d/l, i.e.:

$$K_t = C_1 + C_2\frac{d}{D} + C_3\left(\frac{d}{D}\right)^2 \tag{4}$$

where

$$C_1 = \frac{1+5.4\frac{d}{l}}{1+1.7\frac{d}{l}} \tag{5}$$

$$C_2 = \frac{1+862.7\frac{d}{l}}{1+278.2\frac{d}{l}} \tag{6}$$

$$C_3 = \frac{1+37.3\frac{d}{l}}{1-4.6\frac{d}{l}} \tag{7}$$

The constants in Eqs (5) to (7) were determined by post-processing the FE solutions being calculated numerically by employing a conventional least-squares fitting procedure. Tab. 5 confirms that this simple approach allowed us to derive a very effective and simple analytical tool suitable for estimating K_t in metallic wires weakened by semi-ellipsoidal pits. According to Tab. 5, the correlation coefficient between Eqs (4) to (7) and the numerical simulations was seen to be equal to 0.995 (with a standard deviation of 0.024), this returning an absolute value of the error well below 4%.

In what follows, the analytical tools being reviewed and derived in the present section – i.e., Eq. (1) and Eqs (4) to (7), respectively -will be used in conjunction with the TCD to attempt to estimate fatigue lifetime of high-strength metallic wires containing corrosion pits.

3. Fundamentals of the Theory of Critical Distances

The different formalisations of the TCD are based on the assumption that fatigue damage in notched metallic components can be quantified accurately provided that a specific material length scale parameter is somehow incorporated into the stress analysis[15, 47-49]. In this setting, this critical distance is treated as an intrinsic material property and its value is closely related to the size of the dominant source of microstructural heterogeneity[47]. Another important aspect is that, in its simplest formulation, the TCD performs the fatigue assessment of notched/cracked ductile metals by directly post-processing the local stress fields determined by using a linear-elastic constitutive law[15, 47].

Historically, the TCD was first devised to estimate fatigue strength in the high-cycle fatigue regime[47-53], with the required critical distance being calculated - after the advent of Linear Elastic Fracture Mechanics (LEFM) - according to the following well-known formula[54]:

$$L = \frac{1}{\pi}\left(\frac{\Delta K_{th}}{\Delta \sigma_0}\right)^2 \tag{8}$$

In Eq. (8) ΔK_{th} is the threshold value of the stress intensity factor range and $\Delta \sigma_0$ is the range of the plain material fatigue (endurance) limit.

Taking as a starting point this classic formulation of the TCD, in 2007 Susmel and Taylor[16] extended the use of this powerful theory back to the medium-cycle fatigue regime. This was done by forming the hypothesis that, for a given material, the material critical length increases as the number of cycles to failure, N_f, decreases. According to this assumption, the way the critical distance changes with N_f was proposed to be modelled via a simple power law, i.e.[16, 47]:

$$L_M(N_f) = A \cdot N_f^B \tag{9}$$

In Eq. (9) A and B are material fatigue constants to be determined either by using conventional material fatigue properties or by running appropriate experiments[16, 47].

In situations of practical interest, the TCD can be applied in different forms[15, 53] as schematically shown in Fig. 4. The Point Method (PM) assumes that the effective stress, $\Delta \sigma_{eff}$, to be used to perform fatigue assessment is equal to the range of the linear-elastic stress determined at a given distance from the assessed stress concentrator (Fig. 4b). According to the LM instead, $\Delta \sigma_{eff}$ is calculated by averaging the local linear-elastic stress over a line radiating from the notch tip (Fig. 4c). It is important to highlight here that, to apply both the PM and LM, the reference straight-

line used to estimate $\Delta\sigma_{eff}$ (i.e., the so-called focus path[15]) is assumed to emanate from the crack initiation point, with this direction being perpendicular to the component surface at the hot-spot itself[49]. According to this simple and intuitive geometrical rule, in the presence of conventional U- and V-notches loaded either in cyclic tension or in cyclic bending, obviously, the focus path invariably coincides with the notch bisector (as for the notches sketched in Fig. 4).

Turning back to the different formalisations of the TCD, the Area Method (AM) postulates instead that the effective stress range can be calculated also by averaging the local linear-elastic stresses over a semi-circular area centred at the tip of the crack/notch under investigation (Fig. 4d). According to the above definitions, $\Delta\sigma_{eff}$ can then be determined mathematically as follows[15, 47, 53]:

$$\Delta\sigma_{eff} = \Delta\sigma_y\big(\theta = 0°, r = L_M\big(N_f\big)/2\big) - \text{Point Method (PM, Fig. 4b)} \tag{10}$$

$$\Delta\sigma_{eff} = \frac{1}{2L_M(N_f)} \int_0^{2L_M(N_f)} \Delta\sigma_y\,(\theta = 0°, r) \cdot dr - \text{Line Method (LM, Fig. 4c)} \tag{11}$$

$$\Delta\sigma_{eff} = \frac{4}{\pi[L_M(N_f)]^2} \int_{-\pi/2}^{\pi/2} \int_0^{L_M(N_f)} \Delta\sigma_1\,(\theta, r) \cdot r \cdot dr \cdot d\theta - \text{Area Method (AM, Fig. 4d)} \tag{12}$$

To conclude this brief overview of the different definitions suitable for determining the effective stress, it is worth observing here that there is also a three-dimensional version of the TCD - known as the Volume Method (VM) - that calculates $\Delta\sigma_{eff}$ by averaging the local linear-elastic stresses in a hemisphere centred at the tip of the stress concentrator being assessed[55].

These different definitions for the range of the effective stress make it evident that employing the AM and VM is very laborious, while using either the PM or LM is instead very straightforward. This explains the reason why when it comes to performing the fatigue assessment of real notched/cracked components, the PM and LM are always preferred over the other two methods. Having said that, with the aim of proposing a simple approach suitable for rapid fatigue design of pitted/cracked/damaged metallic wires, in what follows the TCD will then be used solely in the forms of the PM and the LM.

In order to use the TCD in situations of practical interest to estimate fatigue lifetime of notched metals, the first problem to be addressed is the determination of material fatigue constants A and B in Eq. (9). Owing to the specific nature of the design problem being addressed in the present paper, for the fatigue assessment of metallic wires containing cracks/corrosion pits, the L_M vs. N_f relationship will be calibrated by using both static and fatigue material properties.

To understand how this calibration procedure works in practice, consider the SN curve for a standard structural steel reported in Fig. 4e. This curve is assumed to be determined experimentally by testing, under a given value of the load ratio, R, plain (i.e., un-notched) specimens. As per the standard log-log schematisation that is usually adopted to describe the fatigue behaviour of engineering metals[47], this SN curve can be expressed mathematically as:

$$\sigma_a^k \cdot N_f = \sigma_0^k \cdot N_0 \qquad (13)$$

where $\sigma_0 = \Delta\sigma_0/2$ is the amplitude of the endurance limit at N_0 cycles to failure and k is the negative inverse slope.

According to the schematic SN diagram of Fig. 4e, it is also possible to determine the amplitude of the stress, σ_S, at which the parent material breaks statically. This reference stress amplitude is a function of the material ultimate tensile strength, σ_{UTS}, and can be estimated for different values of the load ratio, R, via the following trivial relationship[56]:

$$\sigma_S = \frac{(1-R)}{2} \cdot \sigma_{UTS} \qquad (14)$$

As soon as σ_S is known, it is straightforward to determine from Eq. (13) the corresponding number of cycle to failure, N_S, that is (Fig. 4e):

$$N_S = N_0 \cdot \left(\frac{\sigma_0}{\sigma_S}\right)^k \qquad (15)$$

This simple mathematical framework allows the following calibration conditions to be written explicitly[16]:

$$L_M(N_0) = L = \frac{1}{\pi} \cdot \left(\frac{\Delta K_{th}}{\Delta\sigma_0}\right)^2 \qquad (16)$$

$$L_M(N_s) = L_S = \frac{1}{\pi} \cdot \left(\frac{K_{Ic}}{\sigma_{UTS}}\right)^2 \qquad (17)$$

where L is determined according to definition (8), whereas L_S is the critical distance under static loading which is estimated via the ultimate tensile strength, σ_{UTS}, and the plane strain fracture toughness, K_{Ic}[16, 57-60].

Conditions (16) and (17) can then be used to directly derive constants A and B in the L_M vs. N_f relationship, Eq. (9), obtaining[16]:

$$B = -log\left(\frac{L_S}{L}\right) \cdot \left[log\left(\frac{N_0}{N_S}\right)\right]^{-1} \tag{18}$$

$$A = L \cdot N_0^{-B} \tag{19}$$

As soon as constants A and B are known, the TCD can be employed to estimate fatigue lifetime of notched components provided that a recursive procedure is used to solve this simple design problem. In particular, initially a first attempt value for the number of cycles to failure, $N_{f,i}$, can be assumed arbitrarily, so that, according to Eq. (9), the associated critical distance value takes on the following value:

$$L_M(N_{f,i}) = A \cdot N_{f,i}^B \tag{20}$$

The value for the critical distance estimated according to Eq. (20) can then be used together with one of the strategies reviewed above to determine the corresponding range of the TCD effective stress, $\Delta\sigma_{eff}$ – see Eqs (10) to (12). By so doing, the calculated value for $\Delta\sigma_{eff}$ allows the number of cycles to failure to be obtained directly from the SN curve that models the fatigue behaviour of the parent material, Eq. (13), i.e.:

$$N_{f,j} = N_A \cdot \left(\frac{\Delta\sigma_0/2}{\Delta\sigma_{eff}/2}\right)^k \tag{21}$$

If $N_{f,j}$ is different from $N_{f,i}$, then this simple procedure has to be reapplied by taking $N_{f,i}=N_{f,j}$, with this recursive process being iterated until the design problem reaches its convergence.
In what follows, it will be demonstrated that this particular formalisation of the TCD can be used successfully also to estimate fatigue lifetime of metallic wires containing either corrosion pits or pre-existing defects.

4. Estimating fatigue lifetime of metallic wires containing corrosion pits
As briefly reviewed in the previous section, determining constants A and B in the L_M vs. N_f relationship is the first necessary step that must be taken to use the TCD to estimate fatigue lifetime of notched/cracked metallic materials. In what fallows, this will be done by calibrating

Eq. (9) through same reference experimental material properties that, according to the state-of-the-art knowledge, can be used to assess reliably both the static and the fatigue strength of those high-strength steels that are commonly used to manufacture wires.

Starting from the static properties, as far as K_{Ic} and σ_{UTS} are concerned, Jiang et al.[40] (see also the other relevant references listed therein) recommend to take the plane strain fracture toughness equal to 65.7 MPa·m$^{1/2}$ and the ultimate tensile strength equal to 1835 MPa.

Turning to the fatigue behaviour, as reported by Llorca and Sanchez-Galvez[61], the threshold value of the stress intensity factor range can be estimated under R≥0 via to the following linear equation:

$$\Delta K_{th} = 5.54 - 3.43 \cdot R \qquad [\text{MPa·m}^{1/2}] \tag{22}$$

with the validity of this simple relationship being well-supported also by the ΔK_{th} values collected by Petit et al.[62]

From the experimental results generated by Li, Song and Liu[63] under R>0.4, for those standard steels that are commonly used to fabricate high-strength metallic cables the amplitude of the plain endurance limit, σ_0, at $N_0=2\cdot10^6$ cycles to failure can be taken equal to 128 MPa and the negative inverse slope, k, to 3.7. Therefore, by setting σ_0=128 MPa, k=3.7, σ_{UTS}=1835 MPa and R=0.5 in Eq. (14), it is straightforward to obtain σ_S=459 MPa, with Eq. (15) returning $N_S=17\cdot10^3$ cycles to failure.

These reference materials properties can now be used directly to estimate (under R=0.5) the critical distance value both in the high-cycle, Eq. (16), and in the low-cycle fatigue regime, Eq. (17), obtaining:

$$L_M(N_0 = 2\cdot10^6) = L = \frac{1}{\pi} \cdot \left[\frac{(5.54 - 3.43\cdot0.5)\cdot1000^{0.5}}{2\cdot128} \right]^2 = 0.07 \text{ mm} \tag{23}$$

$$L_M(N_s = 17\cdot10^3) = L_S = \frac{1}{\pi} \cdot \left(\frac{65.7\cdot1000^{0.5}}{1835} \right)^2 = 0.41 \text{ mm} \tag{24}$$

Finally, by taking full advantage of Eqs (18) and (19), it is straightforward to derive material fatigue constants A and B. In particular, the L_M vs. N_f relationship, Eq. (9), for those high-strength steels that are commonly used to manufacture metallic wires can be expressed as follows (for R=0.5):

$$L_M(N_f) = 13.0 \cdot N_f^{-0.36} \text{[mm]} \tag{25}$$

The data listed in Tables 1 to 4 were produced by testing pitted wires under load ratios ranging from 0.4 up to 0.667, with the average value of R being equal to 0.48. Considering such a limited variation for the load ratio, the experimental results being collected were then post-processed by simply applying the TCD along with the fatigue constants derived/estimated for R=0.5 according to the procedure summarised above. It is important to observe here also that a load ratio equal to about 0.5 is considered to be representative[30, 40, 42] of the mean stress effect as it is observed in situations of practical interest (such as, for instance, in bridges).

Having derived the necessary reference material properties, the second aspect to be considered is the definition of a reference error band suitable for assessing the accuracy and reliability of the TCD based approach being proposed in the present paper. To this end, the SN diagram of Fig. 5a summarises all the results that are listed in Tabs 1 to 4, with these results being therefore treated as a homogenous population of experimental data. The scatter band reported in Fig. 5a is delimited by two straight lines corresponding to a probability of survival, P_S, equal to 90% and 10%, respectively. The fatigue curves for P_S equal to 10%, 50% and 90% were determined under the hypothesis of a log-normal distribution of the number of cycles to failure for each stress range level and assuming a confidence level equal to 95%[64, 65]. The estimated, $N_{f,e}$, vs. experimental, N_f, number of cycles to failure diagram reported in Fig. 5b shows the accuracy of the P_S=50% curve determined by post-processing all the results being considered (see Fig. 5b) in predicting the fatigue lifetime of the experimental tests listed in Tabs 1 to 4. This chart shows that the data points fall within an error band of 4. Accordingly, an error band of 3 will be adopted in what follows to quantify the accuracy of the TCD based approach being proposed. This will be done to demonstrate that the use of the proposed methodology results in a higher level of accuracy than the one which is reached by applying the conventional nominal stress based approach as shown in the SN diagram of Fig. 5a.

Before considering pitted cables, to check the validity of the hypotheses that were formed to estimate the calibration constants in the TCD's governing equations, initially the PM was used to estimate the lifetime of wire containing semi-elliptical cracks. The literature data[41, 42] that were used for such a preliminary validation exercise are listed in Tab. 6. The PM was applied by post-processing the linear-elastic stress fields determined analytically along the radial focus path emanating from the apices of the semi-elliptical cracks (i.e., from point A in Fig. 6a). In more detail, by assuming that all the considered defects acted as long-cracks, the necessary stress distributions were determined through the classic LEFM equations[66]. To this end, the required

shape factors were estimated by using the values recommended by Astiz[67] and by Shin & Cai[68]. The experimental, N_f, vs. estimated, $N_{f,e}$, number of cycles to failure diagram reported in Fig. 6b confirms that the assumptions made to estimate the required fatigue properties resulted in estimates falling, on the non-conservative side, well within an error factor of 3.

Having performed this initial check, attention was then focussed on those fatigue results listed in Tabs 1 to 4 and generated by testing metallic wires containing corrosion pits.

As far the stress analysis problem is concerned, initially, the necessary local linear-elastic stress fields were determined numerically by using commercial code ANSYS®. This was done by adopting the same numerical strategy as the one described in Section 2 and used to calculate the SCFs in pitted wires.

As shown in Fig. 7a, the focus path in the presence of semi-ellipsoidal cavities was assumed to emanate radially from the bottom of the cavities themselves. In other words, for this specific pit configuration, the stress-distance curve used to determine $\Delta\sigma_{eff}$ according to both the PM and LM was hypothesised to radiate from that material point experiencing the largest value of the local linear-elastic stress. Turning to the hemispherical cavities, as mentioned earlier, the point experiencing the maximum stress was seen to be, on the surface of the wire, at the edge of the pit (see Fig. 1c). Therefore, for this specific case, according to our previous experience[49], the focus path was assumed to radiate from the hot-spot, with its direction being at about 45° to the surface of the wire. To be precise, according to Fig. 7b, the focus path was taken coincident with the bisector of the angle between the surface of the wire and the flank of the hemispherical cavity.

Using the stress-distance curves determined numerically along the focus paths as defined in Fig. 7, the TCD was then applied together with Eq. (25) in the form of both the PM, Eq. (10), and the LM, Eq. (11). The experimental, N_f, vs. estimated $N_{f,e}$ diagrams reported in Fig. 8 summarise the overall accuracy that was obtained by re-analysing the results listed in Tabs 1 to 4. These charts make it evident that the use of both the PM and the LM resulted in a satisfactory level of accuracy, with the estimates falling within an error factor of 3.

The high level of accuracy obtained by applying the TCD suggests also that fatigue damage in metallic wires containing corrosion pits could be attempted to be quantified by taking full advantage of Neuber's fictitious radius concept[69]. To this end, a possible alternative strategy could be treating corrosion pits as equivalent sharp notches where such stress concentrators are modelled by taking a suitable value for the fictitious root radius. However, while this approach is certainly very appealing from a philosophical point of view, certainly more systematic research work should be done in this area to check the accuracy and reliability of such a design methodology based on the fictitious radius idea.

As briefly discussed above, the estimates summarised in Fig. 8 were obtained by post-processing the local-linear elastic stress fields determined numerically by schematising the corrosion pits either as hemispherical or as semi-ellipsoidal cavities[36-40]. Unfortunately, the real shape of corrosion pits is much more complex than these simplified reference geometries, so that, although very laborious, even the use of complex three-dimensional FE models leads in any case to approximate stress analysis solutions. Further, in situations of practical interest, the stress distributions in the critical regions of the corroded wires could be affected by the presence of multiple pits interacting with each other. However, as observed experimentally[41, 42], in pitted wires cracks are seen to initiate from those pits resulting in the largest localised stress concentration effect. Therefore, in light of the complexity of the local geometries of real pitted wires, it is reasonable to assume that, in any case, accurate estimates can be obtained by simply considering the most damaging pit, with this critical pit being treated as an isolated stress concentrator.

Bearing in mind this important limitations, an attempted was then made to propose a simplified methodology based on the use of one of the equations derived by Glinka and Newport[44]. In particular, according to their well-known analytical approach, the linear-elastic stress field along the bisector of a blunt ($K_t \leq 4.5$) notch having root radius equal to ρ can be expressed as follows (see also Fig. 4a):

$$\Delta\sigma_y(x) = K_t \Delta\sigma_{nom} \left[1 - 2.33\left(\frac{x}{\rho}\right) + 2.59\left(\frac{x}{\rho}\right)^{1.5} - 0.907\left(\frac{x}{\rho}\right)^2 + 0.037\left(\frac{x}{\rho}\right)^3 \right] \tag{26}$$

Owing to its simplicity, this equation can be used directly along with definitions (10) and (11) to estimate the effective stress range, $\Delta\sigma_{eff}$, according to the PM and LM, respectively, obtaining:

$$\Delta\sigma_{eff} = K_t \Delta\sigma_{nom} \left\{ 1 - 2.33\left[\frac{L_M(N_f)}{2\rho}\right] + 2.59\left[\frac{L_M(N_f)}{2\rho}\right]^{1.5} - 0.907\left[\frac{L_M(N_f)}{2\rho}\right]^2 + 0.037\left[\frac{L_M(N_f)}{2\rho}\right]^3 \right\} \tag{27}$$

$$\Delta\sigma_{eff} = \frac{K_t \Delta\sigma_{nom}}{2L_M(N_f)} \left\{ 2L_M(N_f) - \frac{2.33\cdot[2L_M(N_f)]^2}{2\rho} + \frac{2.59\cdot[2L_M(N_f)]^{2.5}}{2.5\rho^{1.5}} - \frac{0.907\cdot[2L_M(N_f)]^3}{3\rho^2} + \frac{0.037\cdot[2L_M(N_f)]^4}{4\rho^3} \right\} \tag{28}$$

The key advantage of these equations (which can easily be solved numerically) is that the elastic peak stress being required can be derived directly from the K_t values estimated according to Eq. (1) for hemispherical pits and according to Eqs (4) to (7) for semi-ellipsoidal pits.

The results obtained by using the PM in the form of Eq. (27) and the LM in the form of Eq. (28) are summarised in the error charts of Fig. 9. The required material properties being used were

again those derived according to the assumptions/reasoning summarised above and used to build also the charts of Figs 6 and 8. The experimental, N_f, vs. estimated, $N_{f,e}$, fatigue lifetime diagrams of Fig. 9 demonstrate that this simplified way of using the TCD is highly successful, with its systematic usage returning estimates that fall mainly within an error factor of 3. In particular, it can be noticed that a larger level of accuracy (and, therefore, conservatism) was reached by applying the TCD in the form of the PM, i.e., by using the simplest formulation of this powerful fatigue assessment theory.

To conclude, it is worth observing that the level of accuracy shown in Figs 8 and 9 was obtained by using material fatigue properties that were either derived from different sources or somehow estimated – see Eqs (22) to (25). Having highlighted this, it is logical to presume that the use of calibration mechanical properties determined experimentally in a rigorous way would have resulted in a higher level of accuracy. However, in spite of this obvious limitation, certainly the obtained level of accuracy (see Figs 8 and 9) is certainly satisfactory, with this confirming that the TCD can be used with confidence also to assess fatigue damage in metallic wires containing corrosion pits.

5. Conclusions

In the present paper, the fatigue behaviour of high-strength steel wires containing corrosion pits was investigated based on a large number of experimental results taken from the literature. According to the state-of-the-art knowledge, the pits were modelled either as semi-ellipsoidal or as hemispherical cavities. The SCFs associated with these pit geometries were determined by solving three-dimensional FE models through commercial software ANSYS®. The K_t values being calculated according to this standard numerical procedure were then post-processed in order to propose simple analytical solutions suitable for being used in situations of engineering interest.

Finally, after making some assumptions to derive the necessary fatigue properties, the TCD was used in the form of the PM and the LM to estimate the fatigue lifetime of high-strength metallic wires containing corrosion pits.

The key outcomes and conclusions from this research work are summarised in the bullet points reported below.

- According to Eq. (1), the SCFs in hemispherical pits can be estimated accurately by simply using those analytical solutions obtained by considering spherical cavities in finite-radius cylinders subjected to remote tension.

- According to Eqs (4) to (7), the SCF in the presence of semi-ellipsoidal pits is a non-linear function of aspect ratios d/l and d/D, with dimensions d, l, and D being defined as shown in Fig. 1.

- Independently of the strategy being adopted to perform the stress-analysis, the linear-elastic TCD applied in the form of the PM and the LM is seen to be successful in estimating fatigue lifetime of steel wires weakened by corrosion pits, with the obtained estimates falling within an error factor of 3. This result is certainly satisfactory, especially in light of the fact that the material properties needed to calibrate the TCD were taken from different sources.

- Fatigue strength of high-strength steel wires containing corrosion pits can be assessed according to the TCD by simply estimating the necessary local stress fields via well-known analytical solutions. For instance, in the present investigation, the classic equation proposed by Glinka & Newport[44] was used. This allows the time and resources needed to estimate fatigue damage in metallic cables containing pits to be reduced markedly.

References

[1] Nakamura S, Suzumura K, Tarui T. Mechanical properties and remaining strength of corroded bridge wires. Struct Eng Int 2004;14(1):50-54.

[2] Anon. Standard Guide for Examination and Evaluation of Pitting Corrosion. ASTM International, ASTM G46-94(2018), West Conshohocken, PA; 2018.

[3] Eubank RA. Stress concentration due to a hemispherical pit at a free surface. J Appl Mech 1954;21:57-62.

[4] Chen GS, Wan K, Gao M, Wei RP, Flournoy TH. Transition from pitting to fatigue crack growth—modeling of corrosion fatigue crack nucleation in a 2024-T3 aluminum alloy. Mater Sci Eng A Struct Mater 1996;219(1):126-132.

[5] Turnbull A, Horner DA, Connolly BJ. Challenges in modelling the evolution of stress corrosion cracks from pits. Eng Fract Mech 2009;76(5):633-640.

[6] Turnbull A, Wright L, Crocker L. New insight into the pit-to-crack transition from finite element analysis of the stress and strain distribution around a corrosion pit. Corros Sci 2010;52(4):1492-1498.

[7] Kondo Y. Prediction of Fatigue Crack Initiation Life Based on Pit Growth. Corrosion 1989;45(1):7-11.

[8] Cerit M, Genel K, Eksi S. Numerical investigation on stress concentration of corrosion pit. Eng Fail Anal 2009;16(7):2467-2472.

[9] Huang Y, Wang C, Tu S, Xuan F, Itoh T. Numerical Investigation of Stress Concentration Factor at Irregular Corrosion Pit Under Tension-Torsion Loading. Proceedings of the ASME 2014 Pressure Vessels and Piping Conference, Anaheim, USA, American Society of Mechanical Engineers, 2014, p. V6A.

[10] Lennon G. Pitting Corrosion: Challenges and Accomplishments. NY Research Press, USA, 2015.

[11] Cerit M. Numerical investigation on torsional stress concentration factor at the semi elliptical corrosion pit. Corros Sci 2013;67:225-232.

[12] Cerit M. Corrosion pit-induced stress concentration in spherical pressure vessel. Thin Wall Struct 2019;136:106-112.

[13] Ji J, Zhang C, Kodikara J, Yang S. Prediction of stress concentration factor of corrosion pits on buried pipes by least squares support vector machine. Eng Fail Anal 2015;55:131-138.

[14] An L, Park YC, Kim H. A Numerical Study of the Tensile Stress Concentration in a Hemi-ellipsoidal Corrosion Pit on a Plate. Int J Steel Struct 2019;19(2):530-542.

[15] Taylor D. The Theory of Critical Distances: a new perspective in Fracture Mechanics. Oxford, UK, Elsevier, 2007.

[16] Susmel L, Taylor D. A novel formulation of the Theory of Critical Distances to estimate lifetime of notched components in the medium-cycle fatigue regime. Fatigue Fract Eng Mater Struct 2007;30(7):567-581.

[17] Susmel L, Taylor D. The Theory of Critical Distances to estimate lifetime of notched components subjected to variable amplitude uniaxial fatigue loading. Int J Fatigue 2011;33(7):900-911.

[18] Louks R, Susmel L. The linear-elastic Theory of Critical Distances to estimate high-cycle fatigue strength of notched metallic materials at elevated temperatures. Fatigue Fract Engng Mater Struct 2015;38:629−640.

[19] Cheng Z, Liao R, Lu W, Wang D. Fatigue notch factors prediction of rough specimen by the theory of critical distance. Int J Fatigue 2017;104:195-205.

[20] Skallerud B, Kyrre Ås S, Ottosen NS. A gradient-based multiaxial criterion for fatigue crack initiation predictionin components with surface roughness. Int J Fatigue 2018;117:384-395.

[21] Herasymchuk OM, Kononuchenko OV, Bondarchuk, VI. Fatigue life calculation for titanium alloys considering the influence of microstructure and manufacturing defects. Int J Fatigue 2015;81:257-264.

[22] Wang R, Li D, Hu D, Meng F, Liu H, Ma Q. A combined critical distance and highly-stressed-volume model to evaluate the statistical size effect of the stress concentrator on low cycle fatigue of TA19 plate. Int J Fatigue 2017;95:8-17.

[23] Larrosa NO, Lopez-Crespo P, Ainsworth RA. An efficient procedure for reducing in-line-inspection datasets for structural integrity assessments. Theor Appl Fract Mec 2018;93:79-87.

[24] Susmel L, Taylor D. Two methods for predicting the multiaxial fatigue limits of sharp notches. Fatigue Fract Engng Mater Struct 2003;26:821-833.

[25] Susmel L. A unifying approach to estimate the high-cycle fatigue strength of notched components subjected to both uniaxial and multiaxial cyclic loadings. Fatigue Fract Engng Mater Struct 2004;27:391-411.

[26] Susmel L, Taylor D. The Modified Wöhler Curve Method applied along with the Theory of Critical Distances to estimate finite life of notched components subjected to complex multiaxial loading paths. Fatigue Fract Engng Mater Struct 2008;31(12):1047-1064.

[27] Susmel L, Taylor D. A critical distance/plane method to estimate finite life of notched components under variable amplitude uniaxial/multiaxial fatigue loading. Int J Fatigue 2012;38:7-24.

[28] Liu B, Yan X. An extension research on the theory of critical distances for multiaxial notch fatigue finite life prediction. Int J Fatigue 2018;117:217-229.

[29] Zhou H, Wen J, Wang Z, Zhang Y, Du X. Fatigue crack initiation prediction of cope hole details in orthotropic steel deck using the theory of critical distances. Fatigue Fract Engng Mater Struct 2016;39(9):1051-1066.

[30] Gorouhi H. Novel fatigue analysis of old metallic bridges through the theory of critical distances (TCD). PhD Thesis, Civil and Environmental Engineering Department, University of Surrey, December 2017 (available at: http://epubs.surrey.ac.uk/845859/)

[31] Taylor D, Barrett N, Lucano G. Some new methods for predicting fatigue in welded joints. Int J Fatigue 2002;24(5):509-518.

[32] Susmel L. Modified Wöhler Curve Method, Theory of Critical Distances and EUROCODE 3: a novel engineering procedure to predict the lifetime of steel welded joints subjected to both uniaxial and multiaxial fatigue loading. Int J Fatigue 2008;30:888-907.

[33] Susmel L. The Modified Wöhler Curve Method calibrated by using standard fatigue curves and applied in conjunction with the Theory of Critical Distances to estimate fatigue lifetime of aluminium weldments. Int J Fatigue 2009;31:197-212.

[34] Al Zamzami I, Susmel L. On the use of hot-spot stresses, effective notch stresses and the Point Method to estimate lifetime of inclined welds subjected to uniaxial fatigue loading. Int J fatigue 2018;117:432-449.

[35] Karakaş Ö, Zhang G, Sonsino CM. Critical distance approach for the fatigue strength assessment of magnesium welded joints in contrast to Neuber's effective stress method. Int J Fatigue 2018;112:21-35.

[36] Lan CM. Study on life-cycle safety assessment methods for parallel wire stay cable. School of Civil Engineering, Harbin Institute of Technology, Harbin, China, 2009 - http://cdmd.cnki.com.cn/Article/CDMD-10213-2009292188.htm

[37] Zheng XL. Research on the fatigue performance of corroded steel wire and evaluation method of fatigue reliability for bridge cables. College of Civil Engineering and Architecture, Zhejiang University, Hangzhou, China, 2018. - http://cdmd.cnki.com.cn/Article/CDMD-10335-1018244275.htm

[38] Hou XD. Experimental study and numerical analysis on fatigue strength of parallel wire based on corrosion classification. College of Civil Engineering, Nanjing Forestry University, Nanjing, China, 2015 - http://cdmd.cnki.com.cn/Article/CDMD-10298-1015809242.htm

[39] Sun CZ. Assessment of safety capability and fatigue life of corroded cable for cable-supported Bridge. College of Civil Engineering, Southeast University, Nanjing, China, 2013 - http://www.wanfangdata.com.cn/details/detail.do?_type=degree&id=Y2511929

[40] Jiang C, Wu C, Jiang X. Experimental study on fatigue performance of corroded high-strength steel wires used in bridges. Constr Build Mater 2018;187:681-690.

[41] Llorca J, Sánchez Gálvez V. Fatigue limit and fatigue life prediction in high strength cold drawn eutectoid steel wires. Fatigue Fract Engng Mater Struct 1989;12(1):31-45.

[42] Jiang JH, Ma AB, Weng WF, Fu GH, Zhang YF, Liu GG, Lu FM. Corrosion fatigue performance of pre-split steel wires for high strength bridge cables. Fatigue Fract Engng Mater Struct 2009;32(9):769-779.

[43] Yan JC. Corrosion of Steel Wire with Corrosion Pit Form Research on the Influence of the Stress Intensity Factor. School of Civil Engineering, Changsha University of Science & Technology, Shangsha, China, 2017 - http://cdmd.cnki.com.cn/Article/CDMD-10536-1018249198.htm

[44] Glinka G, Newport A. Universal features of elastic notch-tip stress fields. Int J Fatigue 1987;9(3):143-150.

[45] Wang QZ. Simple formulae for the stress concentration factor for two-and three-dimensional holes in finite domains. J Strain Anal Eng 2002;37(3):259-264.

[46] Murakami Y. Theory of elasticity and stress concentration. John Wiley & Sons, Chichester, UK, 2016.

[47] Susmel L. Multiaxial Notch Fatigue: from nominal to local stress-strain quantities. Woodhead & CRC, Cambridge, UK, 2009.

[48] Susmel L. The Theory of Critical Distances: a review of its applications in fatigue. Eng Frac Mech 2008;75(7):1706-1724.

[49] Louks R, Gerin B, Draper J, Askes H, Susmel L. On the multiaxial fatigue assessment of complex three-dimensional stress concentrators. Int J Fatigue 2014;63:2014.

[50] Neuber H. Theory of notch stresses: principles for exact calculation of strength with reference to structural form and material. Springer Verlag, Berlin, II Ed. 1958.

[51] Peterson RE. Notch Sensitivity. In: Sines G., Waisman J. L., Editors. Metal Fatigue. New York. McGraw Hill 1959;293-306.

[52] Tanaka K. Engineering formulae for fatigue strength reduction due to crack-like notches. Int J Fracture 1983;22:R39-R45.

[53] Taylor D. Geometrical effects in fatigue: a unifying theoretical model. Int J Fatigue 1999;21:413-420.

[54] El Haddad MH, Topper TH, Smith KN. Prediction of non-propagating cracks. Eng Frac Mech 1979;(3):573-584.

[55] Bellett D, Taylor D, Marco S, Mazzeo E, Guillois J, Pircher T. The fatigue behaviour of three-dimensional stress concentrations. Int J Fatigue 2005; 27:207–221.

[56] Susmel L. On the estimation of the material fatigue properties required to perform the multiaxial fatigue assessment. Fatigue Fract Engng Mater Struct. 2013;36:565–585.

[57] Susmel L, Taylor D. The theory of critical distances to predict static strength of notched brittle components subjected to mixed-mode loading. Eng Frac Mech 2008;75(3-4):534-550.

[58] Susmel L, Taylor D. On the use of the Theory of Critical Distances to predict static failures in ductile metallic materials containing different geometrical features. Eng Frac Mech 2008;75:4410-4421.

[59] Susmel L, Taylor D. The Theory of Critical Distances to estimate the static strength of notched samples of Al6082 loaded in combined tension and torsion. Part I: Material cracking behaviour. Eng Frac Mech 2010;77:452–469.

[60] Susmel L, Taylor D. The Theory of Critical Distances to estimate the static strength of notched samples of Al6082 loaded in combined tension and torsion. Part II: Multiaxial static assessment. Eng Frac Mech 2010;77:470–478.

[61] Llorca J, Sánchez-Gálvez V. Fatigue threshold determination in high strength cold drawn eutectoid steel wires. Eng Frac Mech 1987;26(6);869-882.

[62] Petit J, Sarrazin-Baudoux C, Lorenzi F. Fatigue crack propagation in thin wires of ultra high strength steels. Procedia Engineering 2010;2(1):2317-2326.

[63] Li XL, Song XH, Liu YQ. Investigation on fatigue reliability of high strength galvanized steel wires. China Civil Eng J 1995;28(2):36-43.

[64] Spindel JE, Haibach E. Some considerations in the statistical determination of the shape of S-N cruves. In: Statistical Analysis of Fatigue Data, ASTM STP 744 (Edited by Little, R. E. and Ekvall, J. C.), pp. 89–113, 1981.

[65] Al Zamzami, I., Susmel, L. On the accuracy of nominal, structural, and local stress based approaches in designing aluminium welded joints against fatigue. Int J Fatigue 101 (2), pp. 137-158, 2017.

[66] Anderson TL. Fracture Mechanics: Fundamentals and Applications. CRC Press, Boca Raton, FL, USA, Fourth Edition, 2017.

[67] Astiz MA. An incompatible singular elastic element for two- and three-dimensional crack problems. Int J Fracture 1986;31:105-124.

[68] Shin CS, Cai CQ. Experimental and finite element analyses on stress intensity factors of an elliptical surface crack in a circular shaft under tension and bending. Int J Fracture 2004;129:239-264.

[69] Neuber H. Kerbspannungslehre: Theorie der Spannungskonzentration Genaue Berechnung der Festigkeit. 2nd ed. Berlin, Germany: Springer-Verlag;1958.

List of Captions

Tables

Code	Pit type	$\Delta\sigma_{nom}$ [MPa]	R	N_f [Cycles]	d [mm]	l [mm]	w [mm]	D [mm]
H1		290		3.48×10^5				
H2	Hemisphere	360	0.5	2.14×10^5	0.364	0.728	0.728	4.9
H3		500		9.15×10^4				
H4		640		4.83×10^4				
S1		360		359857				
S2	Semi-ellipsoid	440	0.5	168571	0.246	0.89	0.89	5
S3		520		104861				
S4		360		472341				
S5	Semi-ellipsoid	450	0.4	217172	0.184	4.06	3.36	7
S6		600		85446				
S7		750		51900				
S8		360		263066				
S9	Semi-ellipsoid	450	0.4	140634	0.403	9.93	5.68	7
S10		600		73688				
S11		750		37848				

Table 1. Fatigue results generated by testing corroded steel wires under uniaxial tension loading – data taken from Lan[36], Zheng[37], and Hou[38].

Code	Pit type	$\Delta\sigma_{nom}$ [MPa]	R	N_f [Cycles]	d [mm]	l [mm]	D [mm]
A1-1-1		320		141177			
A1-1-2	Semi-ellipsoid	395	0.55	75599	0.5	8	5
A1-1-3		494		25008			
A1-1-4		626		14247			
A1-2-1		422		75056			
A1-2-2	Semi-ellipsoid	521	0.44	23780	0.5	8	5
A1-2-3		672		17900			
A1-2-4		840		9921			
A1-3-1		520		385115			
A1-3-2	Semi-ellipsoid	640	0.35	135483	0.5	8	5
A1-3-3		840		66102			
A1-3-4		1040		26089			
A2-1		422		74268			
A2-2	Semi-ellipsoid	521	0.44	38124	0.5	3	5
A2-3		672		19518			
A2-4		840		10037			
A3-1		422		78318			
A3-2	Semi-ellipsoid	521	0.44	46700	0.5	5	5
A3-3		672		25597			
A3-4		840		11351			
A4-1		422		57669			
A4-2	Semi-ellipsoid	521	0.44	25279	0.6	5	5
A4-3		672		11815			
A4-4		840		8597			
A5-1		422		115798			
A5-2	Semi-ellipsoid	521	0.44	60300	0.4	5	5
A5-3		672		33921			
A5-4		840		24300			

Table 2. Fatigue results generated by testing corroded steel wires under uniaxial tension loading – data taken from Sun[39].

Code	Pit type	$\Delta\sigma_{nom}$ [MPa]	R	N_f [Cycles]	d [mm]	l [mm]	w [mm]	D [mm]
A-1		520		162711				
A-2	Hemisphere	450	0.4	220664	0.18	0.36	0.36	6.84
A-3		360		464954				
B-1		520		132464				
B-2	Hemisphere	450	0.4	185447	0.26	0.52	0.52	6.7
B-3		360		366536				
C-1		520		73560				
C-2	Hemisphere	450		123274				
C-3		360	0.4	230367	0.39	0.78	0.78	6.6
C-4		270		1072495				
D-1		520		59111				
D-2	Hemisphere	450		103675				
D-3		360	0.4	163443	0.54	1.08	1.08	6.4
D-4		270		586464				
E-1		520		57457				
E-2	Hemisphere	450		83697				
E-3		360	0.4	159810	0.6	1.2	1.2	6.36
E-4		270		510750				
F-1		520		47727				
F-2	Hemisphere	450		67622				
F-3		360	0.4	127807	0.68	1.36	1.36	6.24
F-4		270		306577				

Table 3. Fatigue results generated by testing corroded steel wires under uniaxial tension loading – data taken from Jung et al.[40].

Code	Pit type	$\Delta\sigma_{nom}$ [MPa]	R	N_f [Cycles]	d [mm]	l [mm]	w [mm]	D [mm]
N1				443812	0.48	3.66	1.32	
N2				417042	0.41	3.28	1.54	
N3				452636	0.41	2.88	1.28	
N4				451311	0.37	2.84	1.48	
N5				536748	0.36	2.86	1.28	
N6	Semi-ellipsoid	400	0.667	451869	0.34	2.54	1.34	7
N7				422880	0.34	2.16	1.24	
N8				513352	0.34	2.3	1.08	
N9				416224	0.33	2.18	1.3	
N10				589836	0.32	2.46	1.06	
N11				450168	0.6	6.26	1.32	
N12				206565	0.3	1.86	2.06	
N13				215685	0.53	4.64	1.86	
N14	Semi-ellipsoid	500	0.6	245478	0.47	4.16	1.66	7
N15				245928	0.46	3.76	1.48	
N16				248607	0.37	2.54	1.48	
N17				250104	0.3	1.96	1.38	

Table 4. Fatigue results generated by testing corroded steel wires under uniaxial tension loading – data taken from Yan[43].

Finite Element Analyses						Eqs (4) to (7)				Error
d [mm]	l [mm]	d/D	d/l	D [mm]	K_t	C_1	C_2	C_3	$K_{t,e}$	[%]
0.246	0.89	0.049	0.276	5	1.73	1.696	3.074	41.663	1.75	1.1
0.184	4.06	0.026	0.045	7	1.21	1.156	2.947	3.399	1.24	2.1
0.403	9.93	0.058	0.041	7	1.30	1.140	2.930	3.091	1.32	1.8
0.5	8	0.100	0.063	5	1.59	1.209	2.987	4.675	1.55	2.5
0.5	3	0.100	0.167	5	2.07	1.481	3.057	30.929	2.10	1.0
0.5	5	0.100	0.100	5	1.75	1.316	3.028	8.759	1.71	2.5
0.6	5	0.120	0.120	5	1.93	1.369	3.040	12.223	1.91	1.2
0.4	5	0.080	0.080	5	1.58	1.261	3.011	6.304	1.54	2.4
0.48	3.66	0.069	0.131	7	1.63	1.397	3.045	14.851	1.68	2.5
0.41	3.28	0.059	0.125	7	1.58	1.381	3.042	13.324	1.61	1.5
0.41	2.88	0.059	0.142	7	1.65	1.424	3.049	18.283	1.67	0.9
0.37	2.84	0.053	0.130	7	1.59	1.395	3.045	14.623	1.60	0.5
0.36	2.86	0.051	0.126	7	1.57	1.384	3.043	13.528	1.58	0.5
0.34	2.54	0.049	0.134	7	1.59	1.403	3.046	15.596	1.59	0.3
0.34	2.16	0.049	0.157	7	1.69	1.459	3.054	24.903	1.67	1.3
0.34	2.3	0.049	0.148	7	1.65	1.437	3.051	20.356	1.63	1.0
0.33	2.18	0.047	0.151	7	1.66	1.445	3.052	21.887	1.64	1.4
0.32	2.46	0.046	0.130	7	1.57	1.394	3.045	14.571	1.56	0.6
0.6	6.26	0.086	0.096	7	1.56	1.305	3.025	8.183	1.62	3.7
0.3	1.86	0.043	0.161	7	1.69	1.468	3.055	27.188	1.65	2.6
0.53	4.64	0.076	0.114	7	1.59	1.354	3.037	11.085	1.65	3.4
0.47	4.16	0.067	0.113	7	1.56	1.351	3.036	10.856	1.60	2.7
0.46	3.76	0.066	0.122	7	1.59	1.375	3.041	12.724	1.63	2.4
0.37	2.54	0.053	0.146	7	1.65	1.432	3.050	19.500	1.65	0.1
0.3	1.96	0.043	0.153	7	1.66	1.449	3.053	22.672	1.62	2.4

Table 5. Accuracy of Eqs (5) to (7) in estimating K_t in wires containing semi-elliptical pits.

Code	$\Delta\sigma$ [MPa]	a [mm]	b [mm]	D [mm]	R	N_f [Cycles]
M1	690.1				0.061	109810
M2	578.1				0.069	164120
M3	387.1				0.52	334620
M4	490.2				0.52	158590
M5	527.1				0.18	171450
M6	583.1				0.49	84780
M7	346.3				0.66	343380
M8	400.8	0.1	1	7	0.34	328080
M9	570.4				0.49	92100
M10	356.5				0.64	376080
M11	441.8				0.47	253800
M12	579.3				0.38	133550
M13	598.4				0.52	103050
M14	446.9				0.49	194330
M15	357.8				0.64	270770

Table 6. Summary of the experimental results[41, 42] generated by testing high strength wires containing semi-elliptical cracks (see also Fig. 6a).

Figures
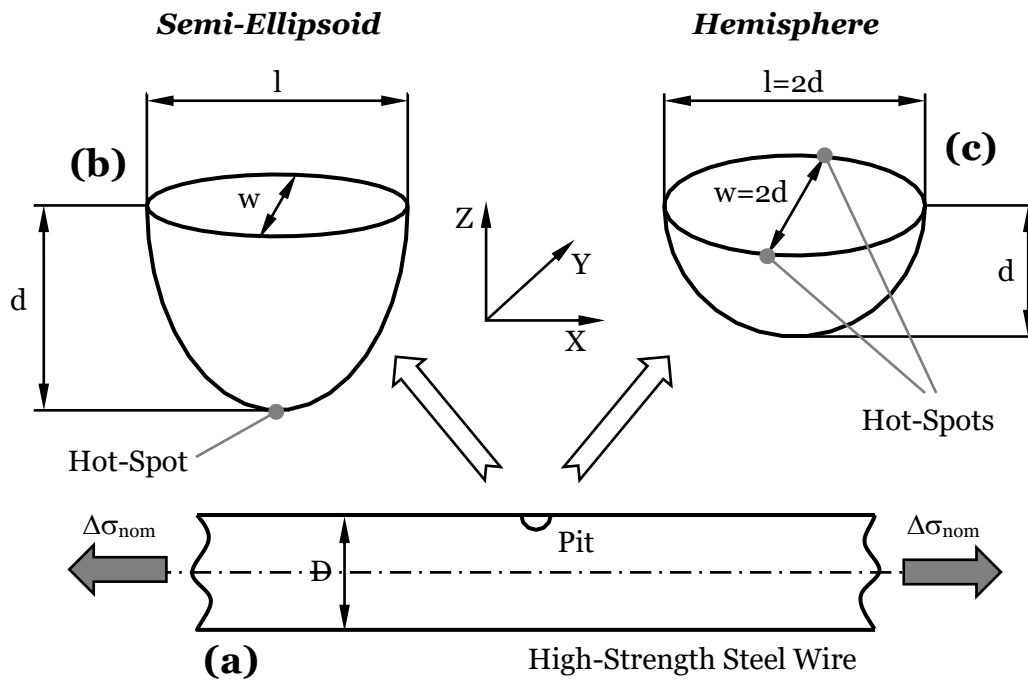
Figure 1. Simplified shapes used to model corrosion pits.

(a)
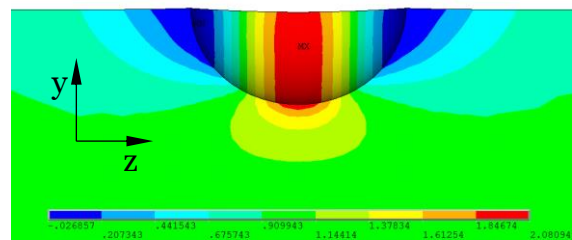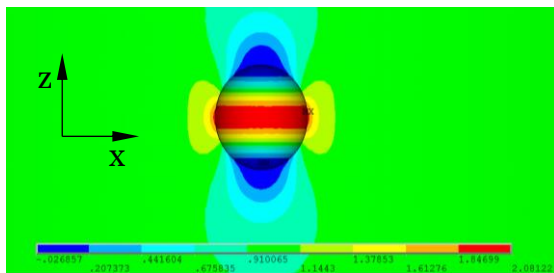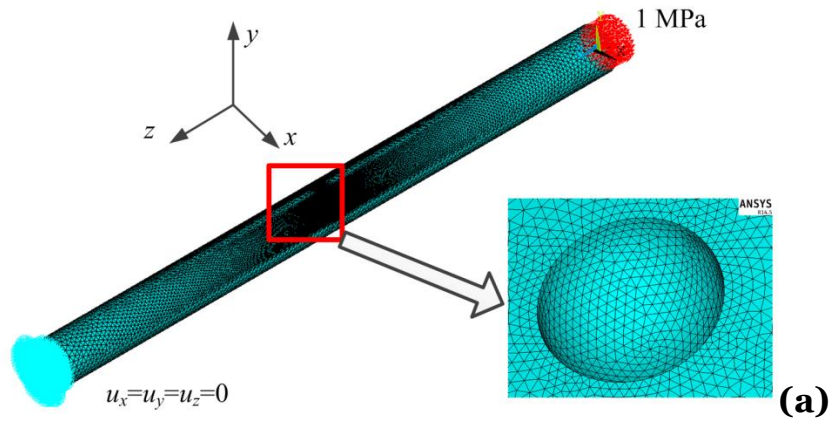
Hemisphere with d=0.18 mm - (b)
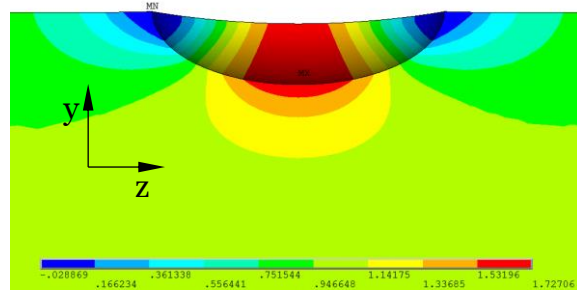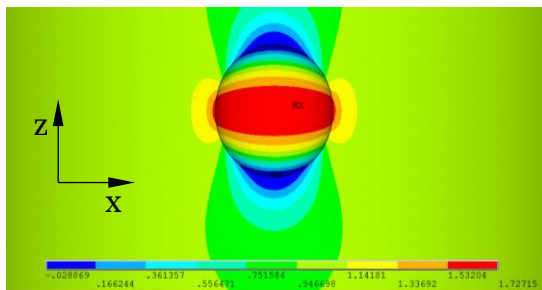
Semi-ellipsoid with d=0.246, l=0.89 mm and w=0.89 mm - (c)

Figure 2. Examples of FE models being solved using commercial software ANSYS® and calculated stress distributions.
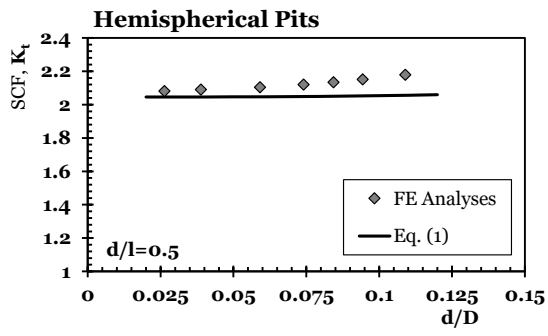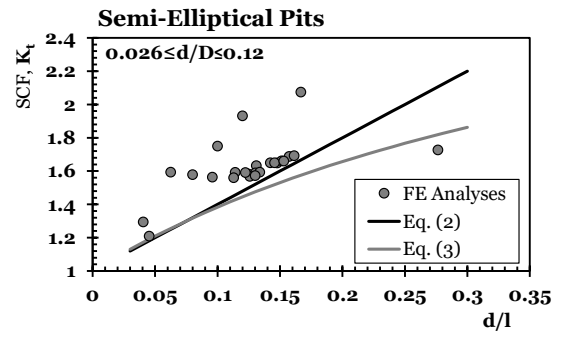
Figure 3. Accuracy of some existing analytical solutions derived by considering other geometrical configurations in estimating K_t in pitted wires.
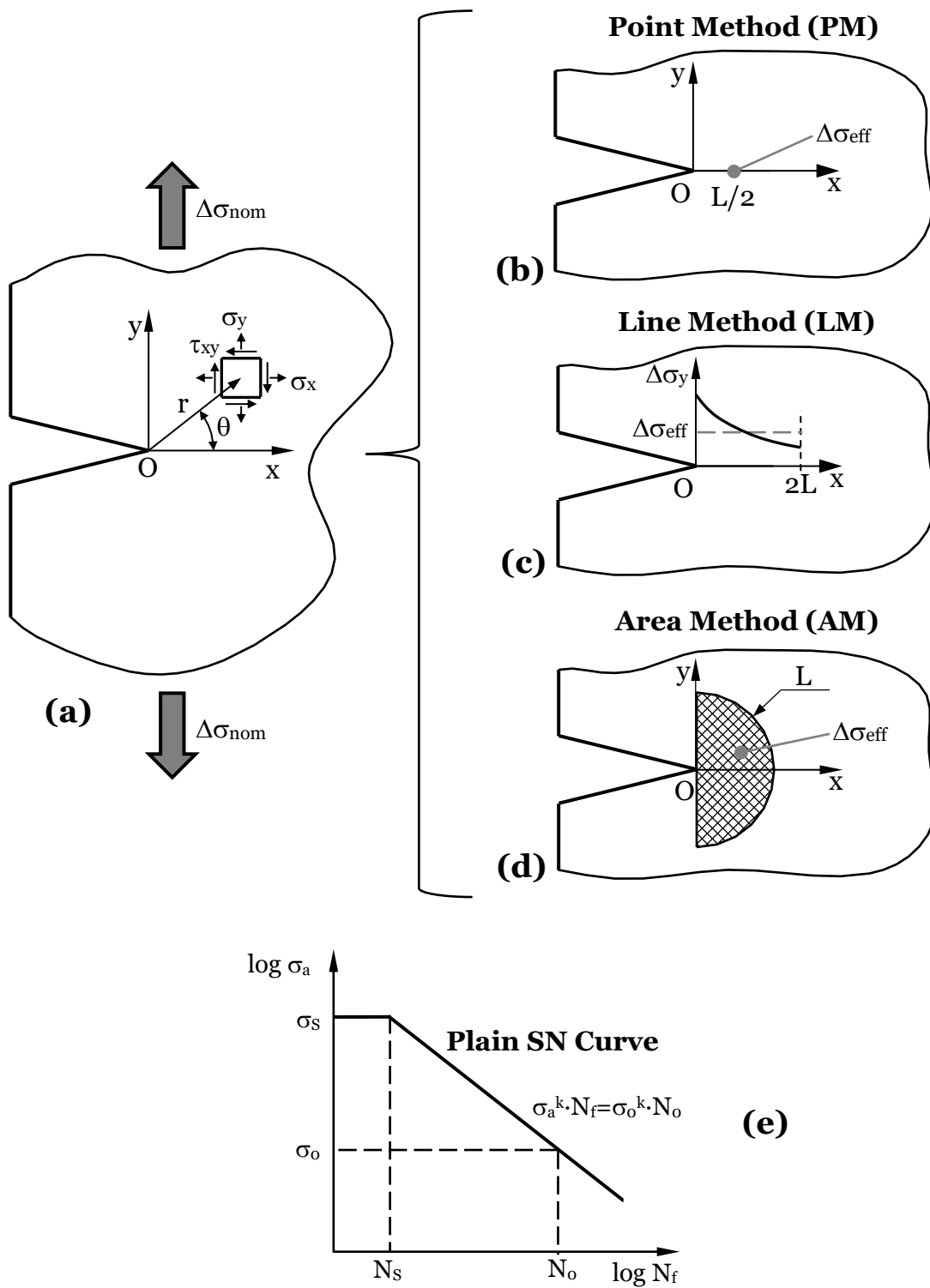
Figure 4. Notched component subjected to fatigue loading (a); the TCD applied in the form of the PM (b), LM (c), and AM (d); plain material fatigue curve (e).

Pitted High-Strength Steel Wires

(a)

Corrosion Pits - Nominal Stress

(b)
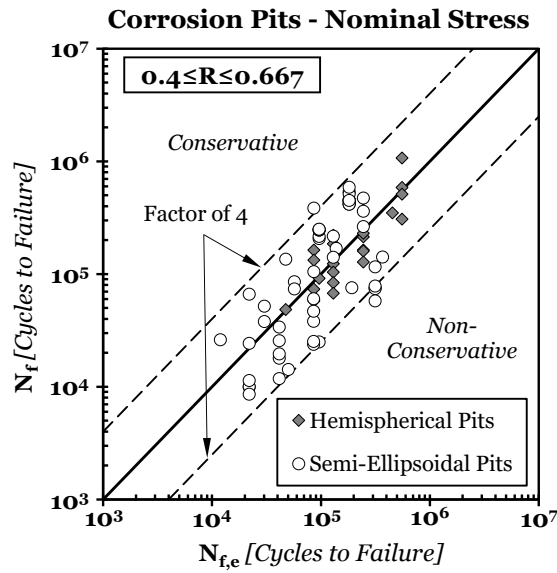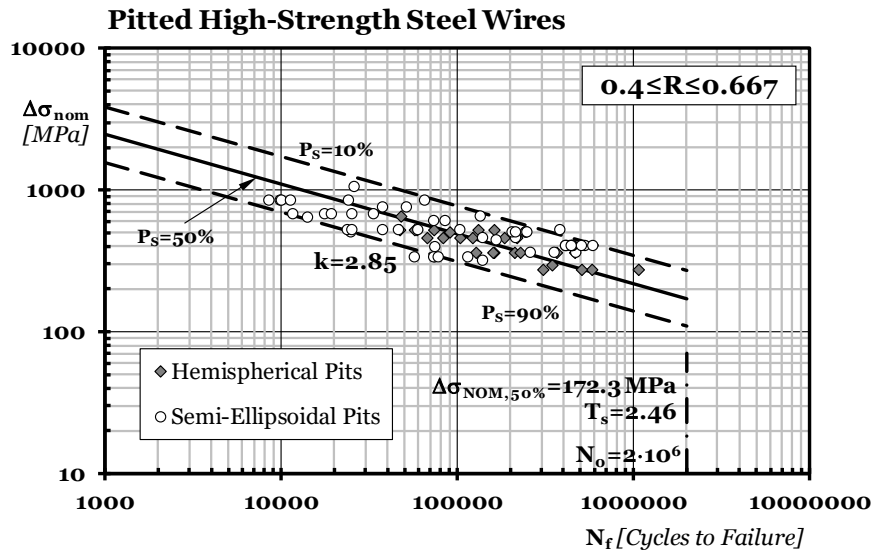
Figure 5. SN curve determined by post-processing the experimental results listed in Tables 1 to 4 in terms of nominal stress range, $\Delta\sigma_{nom}$ (a) and associated error band (b).
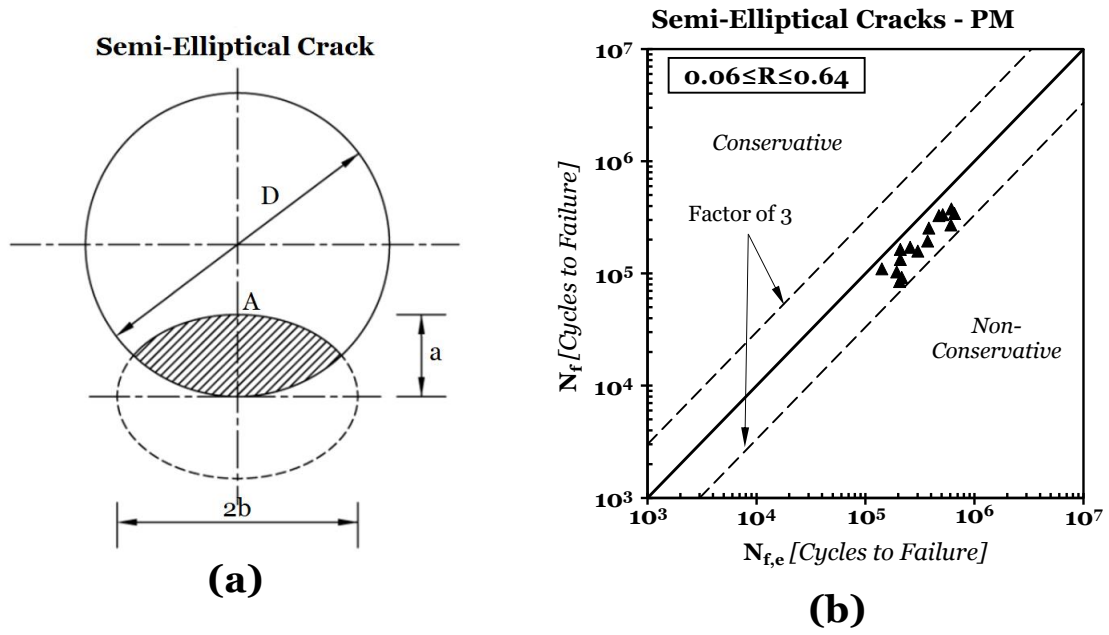
Semi-Elliptical Crack

(a)

Semi-Elliptical Cracks - PM

(b)

Figure 6. Accuracy of the PM in estimating the fatigue lifetime of high-strength steel metallic wires containing semi-elliptical cracks.
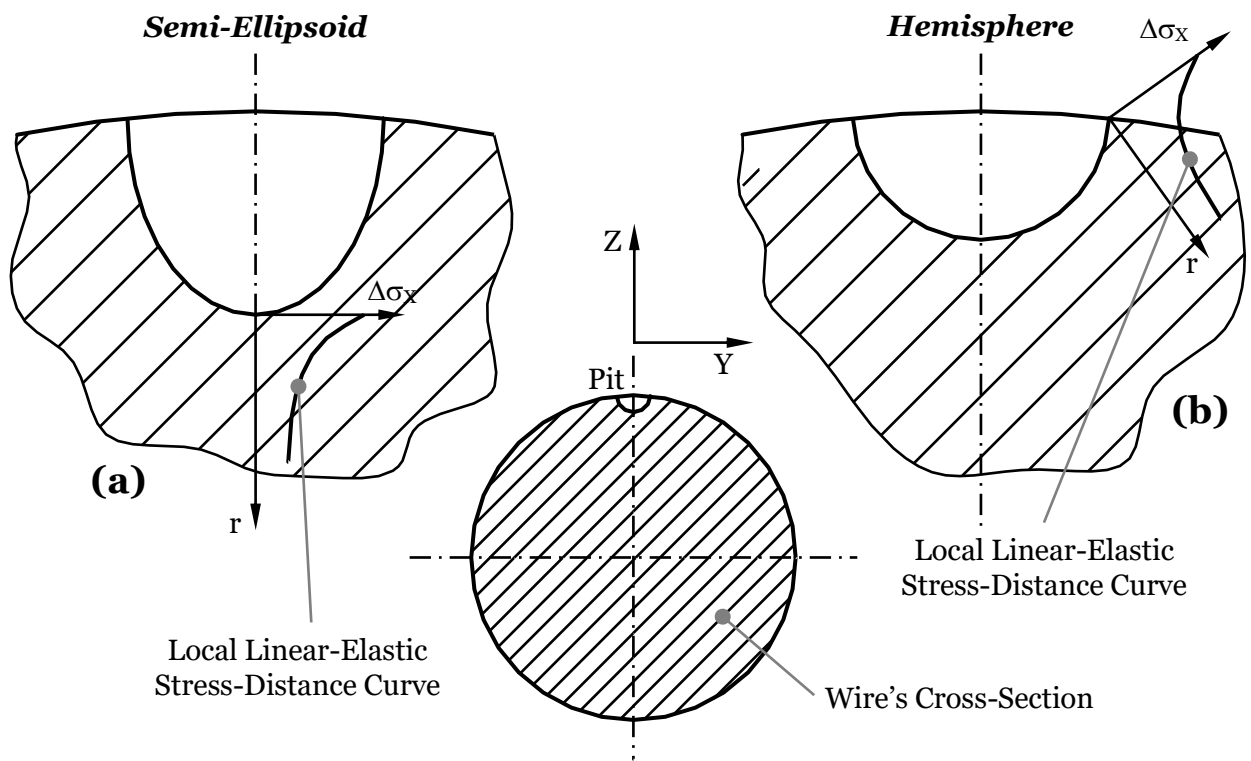
Figure 7. Local linear elastic stress-distance curves determined numerically and used to apply the TCD.
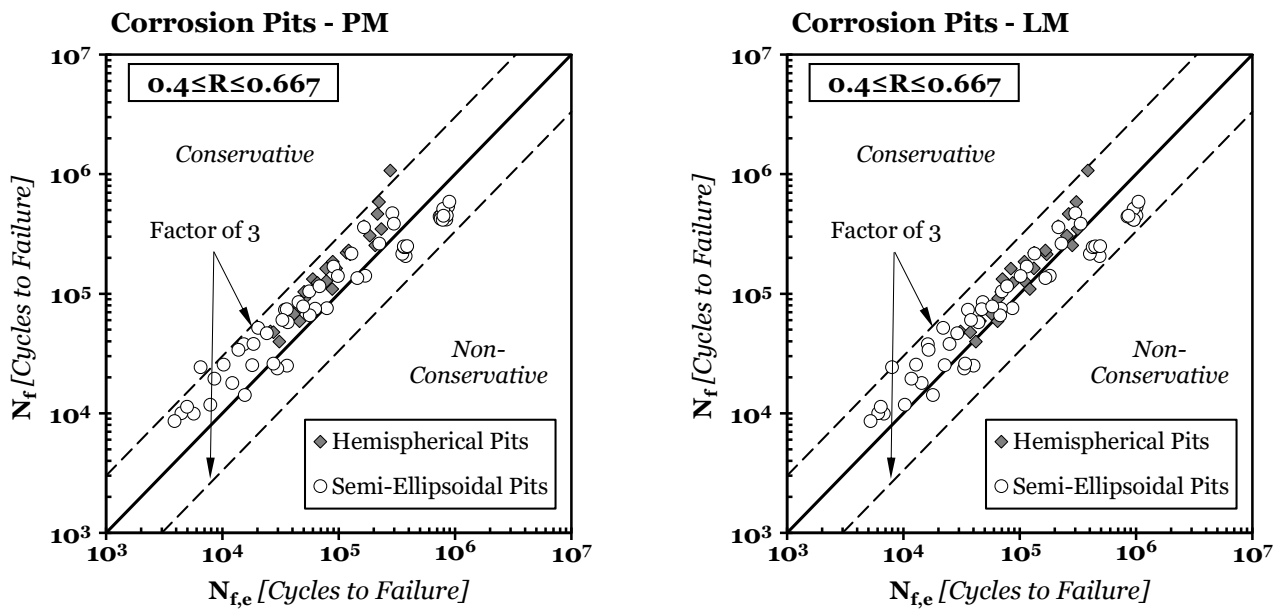
Figure 8. Accuracy of the PM (a) and LM (b) in estimating fatigue lifetime of corroded metallic wires when the required stress fields are determined numerically.
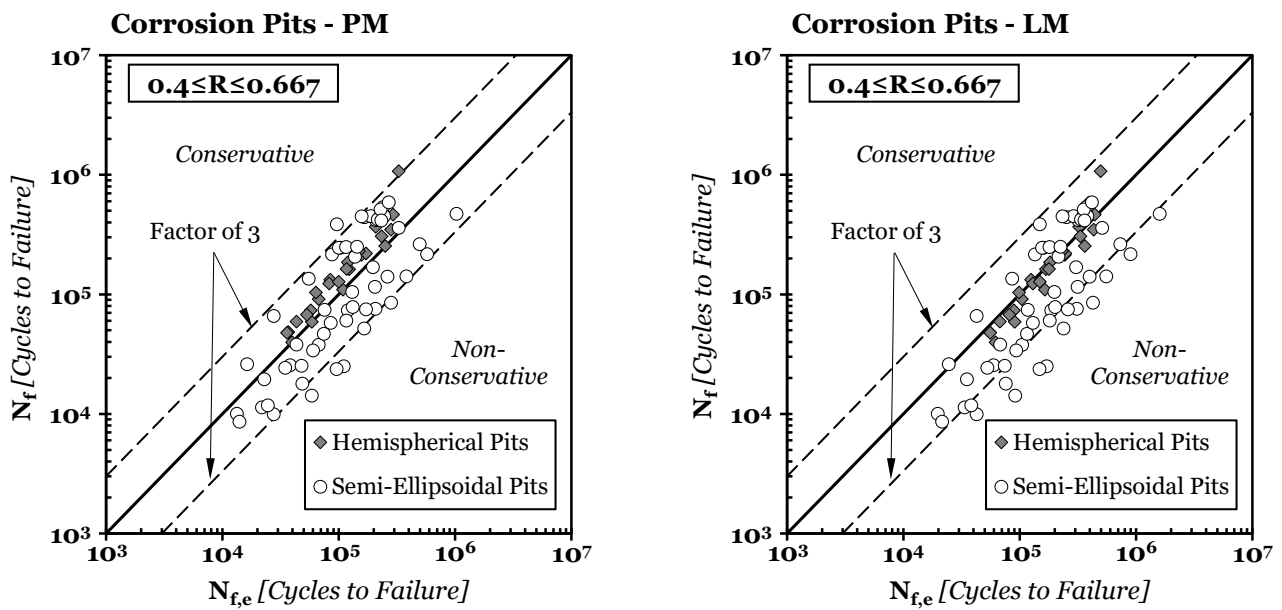

Figure 9. Accuracy of the PM (a) and LM (b) in estimating fatigue lifetime of corroded metallic wires when the required stress fields are determined using Glinka & Newport's analytical solution[44].